# PARAMETRIC STUDY OF A TRIANGULAR CROSS CORRUGATED PLATE

Sharif A.*,  Bağcı Ö. , Ameel B. , De Paepe M and Bokisova L
*Author for correspondence
Department of Flow, Heat and Combustion Mechanics,
University of Ghent, UGent,
Sint-Pietersnieuwstraat 41, 9000 Ghent,
Belgium,
E-mail: Asal.Sharif@ugent.be

## ABSTRACT

The main goal of this study is to investigate the influence of apex angle and Reynolds number on the thermal hydraulic performance of triangular cross corrugated plates. More specifically this work focuses on triangular cross corrugated plate with the orientation angle of 90°. The computational fluid dynamics (CFD) method is used to conduct, three-dimensional simulations for $426 < Re < 2021$ in a periodic unitary cell. The Reynolds Stress model is used as the turbulence model. The numerical results are in a very good agreement with experimental results correlation. They show deviations between $0.8 – 4.84$ %. The highest thermal performances are achieved by the both apex angle of 120° and 90°. The lowest thermal performance is observed by the apex angle of 55°. The heat exchanger with the apex angle of 90° has the highest friction factor. For the Reynolds number lower than 1300, the apex angle of 120° shows the lowest friction factor. However for the Reynolds number higher than 1300, the apex angle of 55° shows the highest hydraulic performance.

## INTRODUCTION

Cross corrugated plate heat exchangers are frequently used in industry for different applications such as air conditioning, electronic cooling and exhaust heat recovery.

The flow in the cross corrugated channel has a complex nature and transition from laminar regime to turbulent regime happens at low range of Reynolds number (100-1500) depending on the geometry [1],[2]&[3].

Computational fluid dynamics (CFD) is an effective numerical method to study the thermal hydraulic characteristics of corrugated channels. Several authors used one or several periodic unitary cells to reduce the computational time [4],[5],[6]&[7].

Different turbulence models are used to simulate the flow in the cross corrugated heat exchangers. For example the k-ω SST and the Reynolds Stress Model (RSM) model are used respectively for the Reynolds numbers in the range of 500-6000 [8]&[9] and 1060-3980 [1].

As it is known from the literature, the most popular corrugation profile that has been studied numerically and experimentally is sinusoidal [1],[2],[3],[10],[11]&[12]. Despite all the efforts done to study the sinusoidal cross corrugated heat exchangers as mentioned above, only a few researchers investigated the performance characteristics of triangular heat exchangers numerically and experimentally. Scott et al. [13], Hall et al. [14] Scott and Lobato [15] and Leung and Probert [16] investigated the performance of triangular cross corrugated heat exchangers experimentally. Zhang [17] investigated numerically the flow and heat transfer for the Reynolds number in range of 100 to 6000 in a triangular cross corrugated heat exchanger with the apex angle of 90°.

The lack of a comprehensive performance study of triangular cross corrugated heat exchangers urge a thorough analysis. In this work, the influence of different apex angles on the heat transfer and pressure drop characteristics will be analysed numerically. The Reynolds number in the range of 426-2021 is considered for this study.

## NOMENCLATURE

| | | |
|---|---|---|
| $A$ | [m²] | area |
| $B$ | [m] | base |
| $cp$ | [J/KgK] | specific heat capacity |
| $D_h$ | [m] | hydraulic diameter |
| $f$ | [-] | friction factor |
| $h$ | [W/m²K] | heat transfer coefficient |
| $j$ | [-] | j factor |
| $k$ | [W/m K] | thermal conductivity |
| $L$ | [m] | flow length |
| $\dot{m}$ | [kg/s] | mass flow rate |
| Nu | [-] | Nusselt number |
| $P$ | [Pa] | pressure |
| $Pr$ | [-] | Prandtl number |
| $\dot{q}$ | [W/m²] | heat flux |
| $\dot{Q}$ | [W] | heat transfer rate |
| $Re$ | [-] | Reynolds number |
| $u$ | [m/s] | velocity in x direction |
| $v$ | [m/s] | velocity in y direction |
| $w$ | [m/s] | velocity in z direction |

Greek symbols

| | | |
|---|---|---|
| α | [°] | angle |
| β | [Pa/m] | non periodic pressure gradient |
| υ | [m²/s] | kinematic viscosity |
| ρ | [kg/m³] | density |
| μ | [kg/ms] | dynamic viscosity |
| Θ | [-] | dimensionless temperature |
| Φ | [-] | general dependent variable |
| γ | [°] | corrugation angle |

Subscripts and Superscripts

| | | |
|---|---|---|
| b | | bulk |

| | |
|---|---|
| $c$ | cross section |
| $f$ | frontal |
| $t$ | turbulent |
| $W$ | wall |
| $ws$ | wetted surface |
| $'$ | fluctuation |
| $*$ | periodic |

## COMPUTATIONAL DOMAIN

A periodic unitary cell used as the computational domain is shown in Figure 1. The geometry parameters of the triangular corrugation are the base (B) and the apex angle (α). The corrugation angle (ɣ) is the angle between two neighbouring plates and is fixed at 90° in this study. The design of experiment method (DoE), allows to obtain the most information from a limited number of test cases. A full factorial sampling plan described by Barrentine [18] is used to investigate the influence of two design parameters: the frontal velocity and the apex angle. Three levels are used for each parameter, resulting in nine simulations (=3²), see Table 1.

## BOUNDARY CONDITIONS AND FUID PROPERTIES

Assumptions of no slip boundary condition (Eq. 1) and constant temperature (333K) for velocity and temperature components are applied to the wall. At the left and right sides of the domain, symmetry conditions are used. This means no flow and scalar flux across the boundary. Normal velocities are set to zero at the symmetry boundary and all other properties just outside the solution domain (i=1), are equal to their values at the nearest node just inside the domain (j=2), see Eq. 2.

$$u = v = 0 \tag{1}$$

$$\Phi_{1,j} = \Phi_{2,j} \tag{2}$$

It is assumed that the flow is fully developed in the computational domain. Therefore, stream wise periodic boundary conditions with constant temperature are imposed in the flow direction, linking the inlet and outlet. This means that the flow field entering the domain is identical to the one leaving it (Eq. 3). Assuming linear pressure drop characteristics in the main flow direction, the pressure drop is calculated from (Eq. 4). Where β is a constant, representing the non-periodic pressure gradient and P* is the periodic pressure. A periodic dimensionless temperature is defined in Eq. 5. The dimensionless temperature of the flow entering the domain is equal to the dimensionless temperature of the flow leaving the domain (Eq. 6).

$$u_{inlet} = u_{outlet} \tag{3}$$

$$P = -\beta x_i + P* \tag{4}$$

$$\theta = \frac{T - T_W}{T_b - T_W} \tag{5}$$
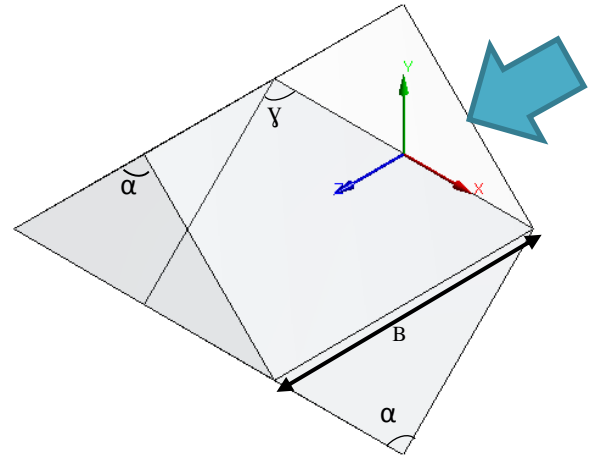
$$\theta_{inlet} = \theta_{outlet} \tag{6}$$



**Figure 1.  A unitary cell**

**Table 1 Levels of design parameters**

| Design parameter | Symbol | Level 1 | Level 2 | Level3 |
|---|---|---|---|---|
| Frontal velocity | uf [m/s] | 0.5 | 1 | 1.5 |
| Apex angle | α [°] | 55 | 90 | 120 |

The fluid considered in this study is air with constant properties (Table 2).

**Table 2 Air properties**

| Density (kg/m³) | Specific heat (J/kg-K) | Thermal conductivity (W/m-k) | Viscosity |
|---|---|---|---|
| 1.225 | 1006.43 | 0.0242 | 1.789e⁻⁵ |

## COMPUTATIONAL MODEL

The steady state three-dimensional numerical simulations of flow and heat transfer in the corrugated channel are obtained with the aid of a commercial CFD code, FLUENT 16.2. It is based on a finite volume technique. The range of Reynolds numbers for the air flow in this study is 426-2021. As it is extensively explained in the introduction section, in this range of Reynolds numbers the flow is not in laminar regime and flow shows the turbulent characteristics. The governing equations are the mass, momentum and energy and are summarized in Eq. 7-9. Where, $(-\overline{\rho \acute{u} \acute{v}})$ and $(-\rho c_p \acute{v} \acute{T})$ are the turbulent stresses and turbulent heat fluxes. Additional turbulence model is required to close these equations. In this study the Reynolds stress model

(RSM) is used. A detailed description of the RSM model is given by Versteeg and Malalasekera, [19].

$$\frac{\partial \rho u}{\partial x} = 0 \tag{7}$$

$$\frac{\partial \rho uv}{\partial y} = -\frac{\partial P}{\partial x} + \frac{\partial}{\partial y}\left[\mu\left(\frac{\partial u}{\partial x} + \frac{\partial v}{\partial y}\right)\right] + \frac{\partial}{\partial y}(-\overline{\rho \acute{u}\acute{v}}) \tag{8}$$

$$\frac{\partial \rho v c_p T}{\partial y} = \frac{\partial}{\partial y}\left[\left(\frac{\mu c_p}{Pr}\frac{\partial T}{\partial y} + (-\rho c_p \acute{v}\acute{T})\right)\right] \tag{9}$$

The discretization of the convective terms in the governing equations is done via a second order upwind scheme. The gradients are evaluated via the least squares cell based method. The pressure gradient in the momentum equations is treated via a second order discretization scheme. Convergence criteria is set to $10^{-5}$ for continuity and velocity components and to $10^{-8}$ for the energy equation. The inlet temperature (mass weighted average temperature at inlet) and velocity (area weighted average velocity) are monitored. It was observed that for some calculation after the aforementioned convergence criteria, the value for inlet temperature and velocity become independent of future calculations. For each simulation, the mass balance is checked. The difference between the air inlet and outlet mass flow rates is within numerical precision. Furthermore, the heat balance is well closed: the heat transfer rate by integrating the local heat flux over the wetted surface is compared with the change of bulk temperature multiplied by the heat capacity rate (Eq. 10). The error on the heat balance is 3.3e-6 %.

$$\dot{Q} = \dot{m}C_p\Delta T \tag{10}$$

## DATA REDUCTION

The Reynolds number is calculated (Eq. 11) based on the velocity in the minimum cross sectional flow area $u_c$ (inlet velocity) and the hydraulic diameter. $\nu$ is the kinematic viscosity of the air. The hydraulic diameter for the unitary cell is defined by Eq. 12. Where $A_c$ is the minimum cross sectional area, L is the flow length and $A_{ws}$ is the wetted surface area.

$$Re = \frac{u_c D_h}{\nu} \tag{11}$$

$$D_h = \frac{4LA_c}{A_{ws}} \tag{12}$$

The mean Nusselt number ($\overline{Nu}$) is obtained from Eq. 13 and Eq. 14, in which $\overline{q_W}$, $k$ and $LMTD$ are respectively the surface averaged wall heat flux, the thermal conductivity of air and the logarithmic mean temperature difference. $T_W$ is the wall temperature, $T_{in,1}$ is the inlet bulk temperature of air and $T_{out,2}$ is the outlet bulk temperature of air.

$$\overline{Nu} = \frac{\overline{q_W}D_h}{k\,LMTD} \tag{13}$$

$$LMTD = \frac{(T_W-T_{out,2})-(T_W-T_{in,1})}{ln(\frac{T_W-T_{out,2}}{T_W-T_{in,1}})} \tag{14}$$

The Colburn j-factor is a dimensionless representation of the convective heat transfer coefficient (Eq. 15). $Pr$ is the Prandtl number.

$$j = \frac{Nu}{Re\,Pr^{1/3}} \tag{15}$$

The Fanning friction factor $f$ is a dimensionless representation of pressure drop. In Eq. 16, $\Delta p$ and $\rho$ are respectively the pressure drop of the unitary cell and the density of air.

$$f = \frac{2\Delta p\,D_h}{\rho L\,u_c^2} \tag{16}$$

## MESH INDEPENDENCE STUDY

Structured meshes consisting of hexahedral and wedge elements are generated. A fine and a coarse mesh are generated for each geometry, with element size of 0.03 and 0.025 mm, respectively. The grid independence study is performed for the highest Reynolds number for each geometry. Furthermore the relative error and grid convergence index (GCI) introduced by Roache [20] for the Colburn and friction factors are reported. The results are shown in Table 3. The maximum differences between both meshes is 0.19% for the Colburn j-factor and 0.46% for the friction factor. The maximum GCI for coarse mesh

**Table 3 Comparison of fine and coarse mesh**

| Re | Fine mesh | | Coarse mesh | | Δj (%) | Δf (%) | j-GCI (%) | f-GCI (%) |
|---|---|---|---|---|---|---|---|---|
| | j | f | j | f | | | | |
| 2026 | 0.007430 | 0.308718 | 0.007436 | 0.308647 | 0.07 | -0.02 | 0.7 | -0.22 |
| 1767 | 0.010296 | 0.468565 | 0.010302 | 0.467517 | 0.05 | -0.22 | 0.52 | -2.16 |
| 1399 | 0.010939 | 0.376597 | 0.010960 | 0.374838 | 0.19 | -0.46 | 1.96 | -4.7 |

is 1.96% for the j-factor and 4.7% for the friction factor. In order to save the computational costs the coarse mesh is used for all

the test cases. Depending on the geometry parameters, 1.3M to 4.5M grid cells are used in this study.

## MODEL VERIFICATION

It is necessary to compare the numerical simulation results with experimental results in order to evaluate the quality of the simulations. To the best of the authors' knowledge, such experimental results corresponding to the geometrical parameters used in this study are not available in literature. Therefore, a CFD model with geometrical parameters identical to the triangular cross corrugated plate used in Scott and Lobato, [13] experimental study is simulated. In Figure. 2, the Nusselt numbers obtained from the CFD simulations and correlation proposed by Scott and Lobato [13] are plotted. As it is seen, the CFD results and experimental results are in good agreement showing deviations between 0.8 – 4.84 %. There is no data available on the accuracy of the experimental correlation.
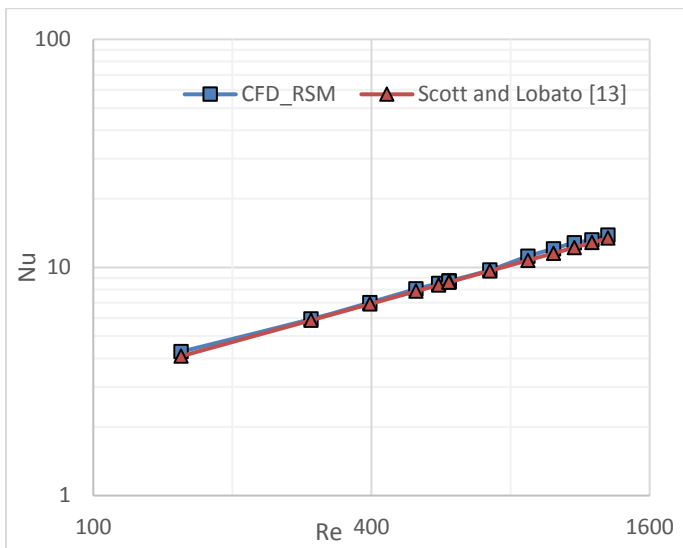


**Figure 2. Comparison between CFD and experimental correlation for Nu number**

## COLBURN J-FACTOR AND FRICTION FACTOR

Figure 3, shows the Colburn j-factor as a function of the Reynolds number for three different apex angles. Increasing the Reynolds number decreases the j-factor. Increasing the Reynolds number increases the Nusselt number. The reason is that the thickness of the thermal boundary layer decreases in both the upper wall and the troughs of the lower wall and the wall temperature gradient increases (see the temperature distribution in mid plane along the flow direction for the case with the angle of 120°, Figure 5) Therefore, the heat transfer enhancement increases by increasing the Reynolds number. The maximum j-factor is obtained at the angle of 90◦ and 120◦. Based on Figure 4, the highest heat transfer coefficient is achieved with the angle of 120◦ and the lowest with the angle of 55◦. At the Reynolds number of 1370, the heat transfer coefficient with the apex angle of 120° is higher than with the apex angle of 90° and 55° respectively, by 34.6% and 121.1%. With observing the temperature distribution of different angles at this Reynolds number (Figure 6) the influence of angle on the thermal

boundary layer is evident. At the angle of 120◦, the thermal boundary layer has the smallest thickness due to less turbulent mixing.
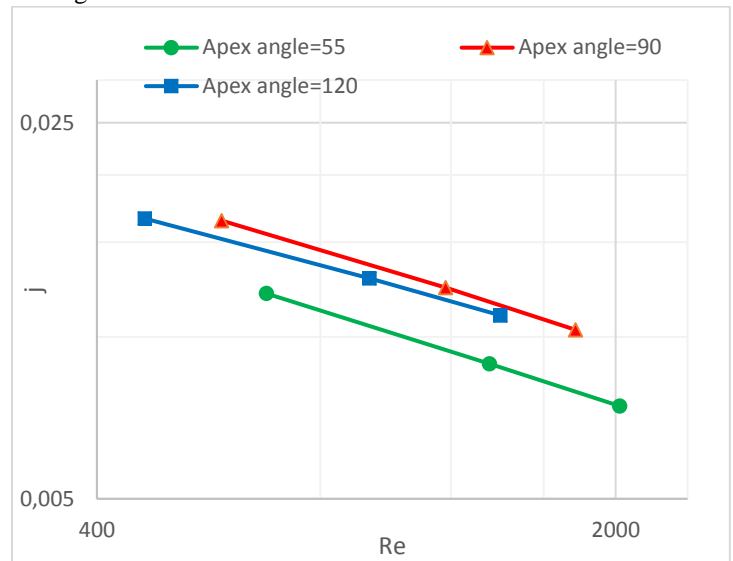


**Figure 3. Colburn j-factor of triangular corrugated plate with different apex angle**

The effect of apex angle on the pressure drop of triangular corrugated plate is shown in Figure 7. The highest pressure drop is related to the apex angle of 120◦ and the lowest is for the apex angle of 55◦. The pressure drop for the apex angle of 120◦ is higher than with the apex angle of 90° and 55° respectively, by 474% and 109%.

Friction factor is a dimensionless representation of the pressure drop. The variation of friction factor by apex angle and Reynolds number is demonstrated in Figure 8.The highest friction factor is obtained by the angle of 90°. For the Reynolds number lower than 1300 the friction factor is higher with the angle of 120° and for the Reynolds number higher than 1300 the friction factor is higher with the angle of 90°. For the same Reynolds number for example 1370, the friction factor with the angle of 90° is higher than with the angle 55° and 120° respectively by 38% and 34%.
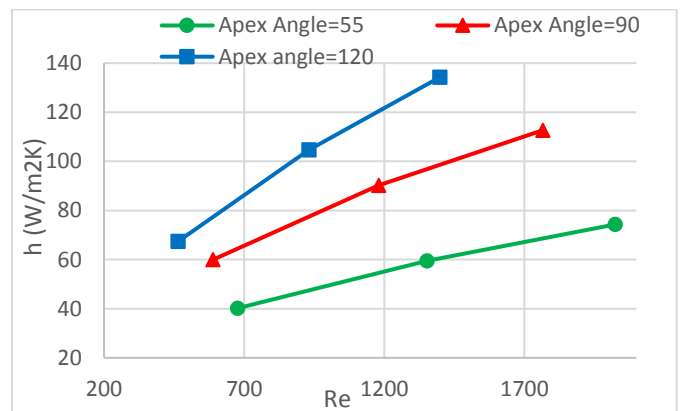


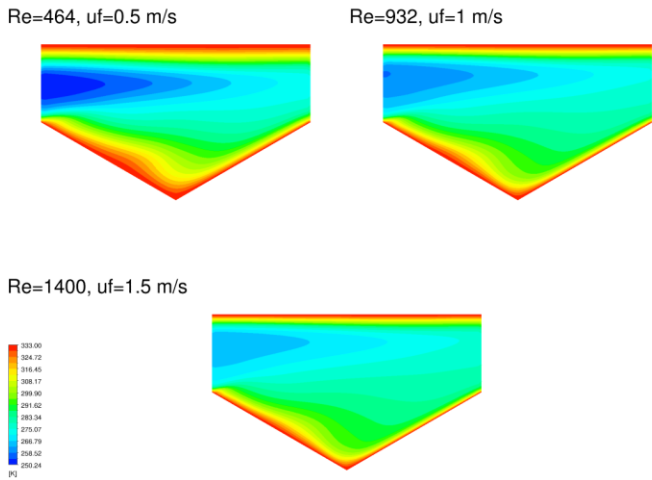**Figure 4. Heat transfer coefficient of triangular corrugated plate with different apex angle**

Re=464, uf=0.5 m/s

Re=932, uf=1 m/s

Re=1400, uf=1.5 m/s

**Figure 5. Temperature distribution in mid plane along the flow direction for the apex angle 120°**
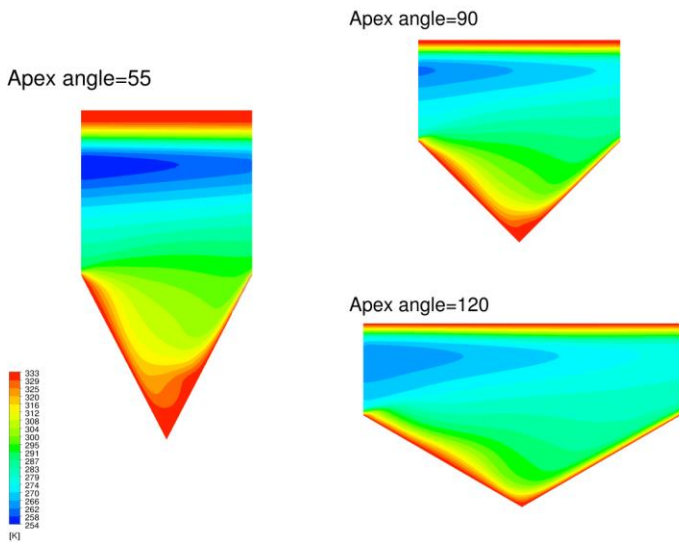
Apex angle=55

Apex angle=90

Apex angle=120

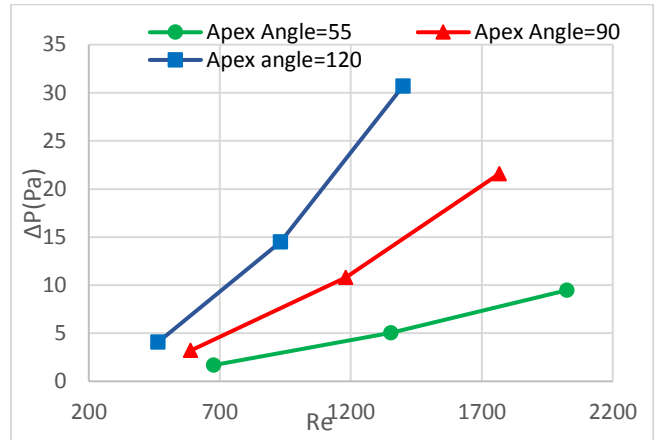**Figure 6. Temperature distribution at Re=1370 for different apex angle**

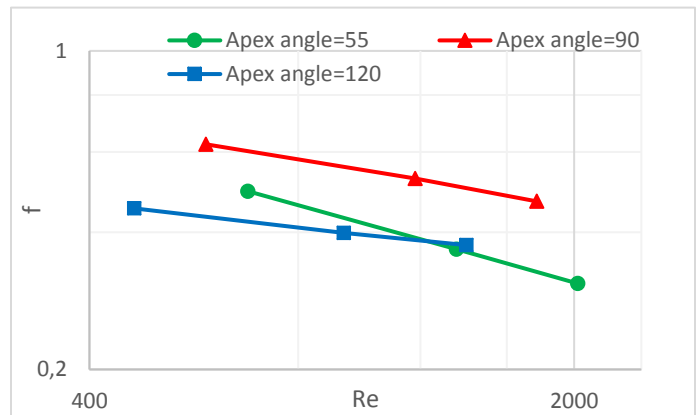**Figure 7. Pressure drop of triangular corrugated plate with different apex angle**

**Figure 8. Friction factor of triangular corrugated plate with different apex angle**

## CONCLUSION

Several three dimensional numerical studies are performed to investigate the influence of the apex angle on the heat transfer and flow characteristics of triangular corrugated plates. It is shown that the numerical and experimental correlation results are in very good agreement. This indicates that RSM model is an appropriate turbulence model for simulating the flow with the Reynolds number in the range of 426-2021 in the cross corrugated channel. Numerical simulations demonstrates that the thermohydraulic characteristics are strongly dependent on the apex angle. Three Nusselt number correlations are proposed for each angle. The highest Nusselt number is achieved by the apex angle of 90° and 120°. In addition, three correlations are proposed for the friction factor with different angles. The heat exchanger with the apex angle of 90° has the highest friction factor. When the Reynolds number is under 1300, the friction factor associated to the apex angle of 120° is the smallest. However, for the Reynolds number higher than 1300, the heat exchanger with the apex angle of 55° shows the lowest friction factor

## ACKNOWLEDGEMENT

## REFERENCES

[1] Shah, R.K. and Wanniarachchi, A.S. [1991]. Plate heat exchanger design theory. *VKI Industrial Heat Exchangers*, *1*.

[2] Focke, W.W., Zachariades, J. and Olivier, I. [1985]. The effect of the corrugation inclination angle on the thermohydraulic performance of plate heat exchangers. International Journal of Heat and Mass Transfer, 28(8), pp.1469-1479.

[3] Liu, F.B. and Tsai, Y.C. [2010]. An experimental and numerical investigation of fluid flow in a cross-corrugated channel. *Heat and Mass Transfer*, *46*(5), pp.585-593

[4] Freund, S., & Kabelac, S. [2010]. Investigation of local heat transfer coefficients in plate heat exchangers with temperature oscillation IR thermography and CFD. *International Journal of Heat and Mass Transfer*, *53*(19), 3764-3781.

[5] Zhang, L. and Che, D. [2011]. Influence of corrugation profile on the thermalhydraulic performance of cross-corrugated plates. *Numerical Heat Transfer, Part A: Applications*, *59*(4), pp.267-296.

[6] Han, W., Saleh, K., Aute, V., Ding, G., Hwang, Y. and Radermacher, R. [2011]. Numerical simulation and optimization of single-phase turbulent flow in chevron-type plate heat exchanger with sinusoidal corrugations. *HVAC&R Research*, *17*(2), pp.186-197.

[7] Etemad, S. and Sundén, B. [2016]. Hydraulic and Thermal Simulations of a Cross-Corrugated Plate Heat Exchanger Unitary Cell. *Heat Transfer Engineering*, *37*(5), pp.475-486.

.

[8] Kanaris, A.G., Mouza, A.A. and Paras, S.V. [2009]. Optimal design of a plate heat exchanger with undulated surfaces. *International Journal of Thermal Sciences*, *48*(6), pp.1184-1195.

[9] Pelletier, O., Strömer, F. and Carlson, A. [2005]. CFD Simulation of Heat Transfer in Compact Brazed Plate Heat Exchangers. *ASHRAE Transactions*, *111*(1).

[10] Blomerius, H., Holsken, C. and Mitra, N.K. [1999]. Numerical investigation of flow field and heat transfer in cross-corrugated ducts. *Journal of heat transfer*, *121*(2), pp.314-321.

[11] Ciofalo, M.I.C.H.E.L.E., Stasiek, J. and Collins, M.W. [1996]. Investigation of flow and heat transfer in corrugated passages—II. *Numerical simulations. International Journal of Heat and Mass Transfer*, 39(1), pp.165-192.

[12] Mehrabian, M.A. and Poulter, R. [2000]. Hydrodynamics and thermal characteristics of corrugated channels: *computational approach. Applied Mathematical Modelling*, 24(5), pp.343-364.

[13] Scott, K., Mahmood, A.J., Jachuck, R.J. and Hu, B. [2000]. Intensified membrane filtration with corrugated membranes. *Journal of Membrane Science*, 173(1), pp.1-16.

[14] Hall, D.W., Scott, K. and Jachuck, R.J.J. [2001]. Determination of mass transfer coefficient of a cross-corrugated membrane reactor by the limiting-current technique. *International journal of heat and mass transfer*, 44(12), pp.2201-2207.

[15] Scott, K. and Lobato, J. [2003]. Mass transport in cross-corrugated membranes and the influence of TiO2 for separation processes. *Industrial & engineering chemistry research*, *42*(22), pp.5697-5701.

[16] Leung, C.W. and Probert, S.D. [1997]. Forced-convective turbulent-flows through horizontal ducts with isosceles-triangular internal cross-sections. *Applied Energy*, *57*(1), pp.13-24.

[17] Zhang, L.Z. [2005]. Numerical study of periodically fully developed flow and heat transfer in cross-corrugated triangular channels in transitional flow regime. *Numerical Heat Transfer, Part A: Applications*, *48*(4), pp.387-405.

[18] Barrentine, L.B. [1999]. *An introduction to design of experiments: a simplified approach*. ASQ Quality Press.

[19] Versteeg, H.K. and Malalasekera, W. [2007]. *An introduction to computational fluid dynamics: the finite volume method*. Pearson Education.

[20] Roache, P.J. [1994]. Perspective: a method for uniform reporting of grid refinement studies. *Journal of Fluids Engineering*, *116*(3), pp.405-413.